How different cells respond to ZIKV infection?

By

Joselyn Landazuri Vinueza

Submitted in partial fulfillment of the requirements for the degree of Master of Art in Biology in the Graduate Division of Queens College of The City University of New York

May 2019

Approved by Mentor: Dr. Zahra Zakeri (Queens College)

Date: _____

TABLE OF CONTENTS

Abstract

The aims of this thesis are to examine which cell lines are vulnerable to Zika virus (ZIKV) infection and to investigate the role of the pro-apoptotic BCL-2 family protein, *BOK* in viral infection. ZIKV, an originally tropical virus, often causes only mild disease but often produces severe neurological problems (1,2). ZIKV attacks neurons, causing apoptosis, cell-cycle arrest, and inhibition of neural progenitor cell differentiation, resulting in cortical thinning and microcephaly (2, - 6). Understanding how ZIKV manipulates cell survival machinery will contribute to the development of anti-viral therapies as well as to our understanding of cell death.

After 24 hours, ZIKV at MOI of 5 infected and killed 15% more Vero cells compared to control cells. However, it did not kill either MDCK or A549 cells by this time. These cell lines, however, are not primary cultures. We therefore asked if Zika would kill primary cells, which were more similar to the *in vivo* target of the virus. Since male and female macrophages differ in their ability to carry out phagocytosis, we also asked whether primary macrophages extracted from male and female mice differ in their response to ZIKV. ZIKV did not alter phagocytosis. However, we found that female macrophages, which phagocytose beads more effectively than male macrophages, produced double amount of viral progeny compared with the male macrophages.

As most of these viruses function by modulation of stress and cell death pathways (7), we also examined a lesser-known member of the BCL-2 family, *BOK*, which promotes apoptosis in response to ER stress (49). We examined how *BOK* affected the course of ZIKV infection. Using $Bok^{-/-}$ (knockout) mouse embryonic fibroblasts and wild-type (WT) cells, we measured cell death by trypan blue assay in infected cells.

ZIKV did not kill either WT or *Bok*$^{-/-}$ cells, suggesting that different types of cells differ in their sensitivity to the virus. To test our hypothesis that the loss of *Bok* (*Bok*$^{-/-}$) would affect the production of ZIKV, we infected WT and *Bok*$^{-/-}$ cells at different times and analyzed the amount of viral RNA (by RT- qPCR), viral proteins (by immunofluorescence) and live virus (by plaque assay). *BOK* impedes virus production as we documented by the increased viral transcription and viral translation in *Bok*$^{-/-}$ cells; however, *Bok*$^{-/-}$ cells cannot release mature virus. Our results indicate that *BOK* is essential for maturation of the virus. Our research will help elucidate the mechanism of ZIKV replication, which we can then use to limit viral replication and cell lethality.

Introduction

Zika Virus (ZIKV)

ZIKV is a newly emerging arbovirus of the *Flaviviridae* family that is related to other medically important flaviviruses, such as Dengue, Yellow Fever, West Nile, Japanese encephalitis and tick-borne encephalitis viruses (8-11). ZIKV was first isolated in 1947 from a sentinel rhesus monkey in Uganda. In 1952, it was found in humans, and it was linked to Zika disease in 1964 (1,12). In 2007 ZIKV gained worldwide attention after an outbreak in Micronesia, French Polynesia, New Caledonia, and more recently Latin America (1, 8, 13).

ZIKV is transmitted primarily by the *Aedes aegypti* mosquito, but unlike other flaviviruses ZIKV can be transmitted by sexual contact, saliva, urine, breast milk, blood transfusion, and by the prenatal route from the mother to the fetus (14-16, 27). Most infections with this virus are asymptomatic, and the majority of symptomatic infections result in a mild and self-limiting febrile illness (13, 18). However, the most alarming feature of ZIKV infection outbreak is that can cause congenital abnormalities and fetal death in pregnant women and serious neurological complications in adults, such as Guillain–Barré syndrome (1, 4, 13, 18-21). The relationship between ZIKV infection and neurodevelopment abnormalities has attracted attention and interest in investigating the mechanism by which these are caused.

ZIKV, like other members of the *Flavivirus* genus, is a positive (+) single-strand RNA virus encoding three structural proteins (core (C), precursor of membrane (prM), and envelope (Env)) and seven non-structural proteins (NS1, NS2A, NS2B, NS3, NS4A, NS4B, NS5) (8, 17, 19). The capsid protein (C) is 13kDa in size, is highly basic, and

complexes with the viral RNA in the nucleocapsid, whereas the outer membrane of the virion is a lipid bilayer containing the viral membrane protein (M) and envelope protein (E). The M protein is expressed as a larger glycosylated precursor protein (prM) (8, 22, 23), whereas the E protein may or may not be glycosylated and mediates cellular attachment, entry, and fusion and is the major target for neutralizing antibodies (24). The nonstructural proteins induce the formation of a membranous network with ER, where viral replication occurs, in addition to controlling viral transcription and replication (19, 20).

Programmed Cell Death

Cell death is an essential process that allows multicellular organisms to achieve a complex internal organization, maintain homeostasis, and define the boundary between self and the environment (25). Apoptosis, a form of programmed cell death that occurs during physiological and pathological conditions, is an important host defense mechanism against intracellular pathogens, such as viruses (26-28). Accordingly, viruses have evolved ways to prevent premature death of infected cells, thereby facilitating virus replication, production of progeny, or persistence (19, 26, 29). Apoptosis can be triggered by extracellular stimuli, such as tumor necrosis factor alpha (TNF-α), Fas ligand, or nutrient depletion, (extrinsic apoptosis) or by intracellular stresses, such as endoplasmic reticulum (ER) stress, hypoxia, or DNA damage (intrinsic apoptosis) (30-32). Viruses regulate apoptosis using different mechanisms; most viruses encode proteins to suppress apoptosis, while some RNA viruses trigger apoptosis to permit release and spreading of virus (26, 29, 33).

The proteins of B cell lymphoma-2 (BCL-2) family are key regulators of the intrinsic apoptotic pathway (30, 34). They are located predominantly on the mitochondria where the critical decision point, cytochrome *c* release, is regulated (35). The members of the family comprise both anti-apoptotic (Bcl-2, Bcl-x_L, Bcl-w, Mcl-1 and A1) and pro-apoptotic (BAX, BAK, and BOK) proteins (28, 30, 32). The fate of a cell depends on the balance of amounts of members of the BCL-2 family of proteins through a dynamic process by which cellular signaling can modulate the expression of pro- or anti-apoptotic proteins to tip the equilibrium towards survival or death (34, 36). When the balance favors death, the oligomerization of pro-apoptotic effector proteins on the outer mitochondrial membrane leads to mitochondrial outer membrane permeabilization and cytochrome *c* release. This triggers the activation of a cascade of caspases that cleave downstream substrates leading to cell death (36).

Endoplasmatic reticulum (ER) stress

Many viruses depend on the extensive membranous network of the ER for their translation, replication, and packaging (19, 37). This is the case of the *Flaviviruses,* the life cycle of which depends on the ER; they are therefore called endoplasmic reticulum tropic (ER-tropic) viruses (45, 41, 37).. The production of viral progeny in the ER represents a stress condition to the host cell (37) that disrupts ER homeostasis and triggers the unfolded protein response (UPR) (19,37). To adapt to the stress, three branches of the UPR, protein kinase RNA-like ER kinase (PERK), inositol-requiring protein 1α (IRE1α) and activating transcription factor 6 (ATF6) are activated to transiently inhibit protein synthesis and restrict the consumption of nutrients and energy, to enhance cell survival and restore homeostasis (19, 39, 40). Prolonged ER stress leads

to cell death through apoptosis, presumptively with the biological goal to limit translation of viral RNAs (19, 42). Infection by an ER-tropic virus disrupts the normal ER function, and then ER stress is induced (19, 43).

In unstressed cells, the major ER chaperone binding-immunoglobulin protein (BIP), also called 78 kDa glucose-regulated protein (GPR78), binds to the ER-oriented parts of PERK and IRE1α and keeps them in a monomeric inactive state (3, 24, 38, 40). Accumulation of unfolded proteins in ER lumen triggers dissociation of GRP78/Bip from the sensors and activates both PERK and IRE1α and facilitates activation by dimerization (or oligomerization) followed by trans(auto) phosphorylation and ATF6 is translocated to the Golgi apparatus and subsequent activation (1, 39, 41). Phosphorylated PERK phosphorylates the α-subunit of eukaryotic translation initiation factor 2 (eIF2α). Phosphorylated eIF2α (phospho-eIF2α) promotes translation of activating transcription factor 4 (ATF4) to express ER chaperones. Activating transcription factor 4 (ATF4) links PERK and apoptosis or autophagy and is essential for the up-regulation of many ER stress-related genes including autophagy related protein (ATG12) and CHOP, which participate in induction of autophagy. Furthermore, ATF4 and CHOP induce the expression of *GADD34*, which serves to direct feedback dephosphorylation of eIF2α-P thereby acting as a negative feedback loop to restore protein translation. IRE1α is activated by a process similar to that of PERK; it dimerizes or oligomerizes to induce autophosphorylation. IRE1 facilitates cytosolic splicing of X-box binding protein 1 (*XBP1)* mRNA, allowing translation of active XBP1s, which enhances transcriptional expression of genes that participate in protein folding, degradation of unfolded or misfolded proteins, and membrane expansion and renewal. In a third pathway, ATF6 is

translocated from the ER membrane to the Golgi where it is proteolytically cleaved. The N-terminal ATF6 fragment, which contains a basic-leucine zipper domain, translocate to the nucleus and induces the expression of target genes involved in the folding and trafficking of proteins slated for the secretory pathways (1, 37-39). These relationships are illustrated in Text Figure a.

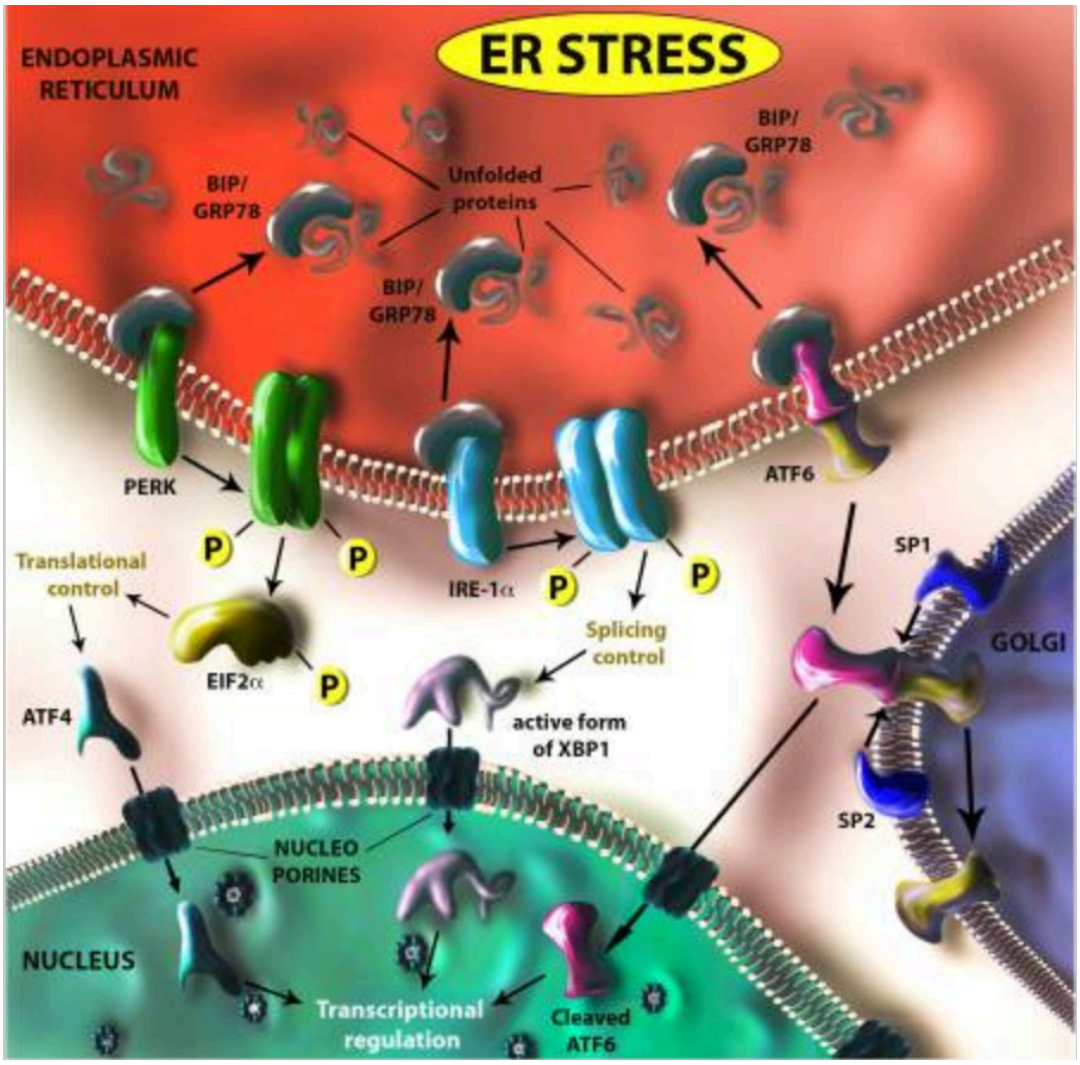

Figure a. The pathways of ER stress. From: Alfano, Christian et al. 2019. The Unfolded Protein Response: A Key Player in Zika Virus-Associated Congenital Microcephaly. Front Cell Neurosci. **13**: 94 (1).

Viruses can manipulate the programs of cell-induced stress to promote viral replication (19, 26). ZIKV may trigger ER stress and upregulate the UPR, especially the PERK stress sensor (1,38). Activation of PERK has been associated with the impairment of ZIKV-infected human neural stem cells (hNSCs) and embryonic mouse brains, presumptively contributing to microcephaly (46).

Here, we assessed ZIKV cell tropism in the different cell lines to investigate which cells are especially vulnerable to ZIKV infection. We also investigated whether ZIKV benefits from ER stress to regulate viral replication. In particular, we investigated whether the pro-apoptotic protein BOK, which induces apoptosis in response to ER stress (5,7), is required for ZIKV life cycle. Therefore, the better understanding of the possible mechanisms and *BOK* pathway involved in cell program death during ZIKV will provide a useful perspective for developing an effective strategy for controlling ZIKV in the future.

Materials and Methods

Cell culture and treatments

Adherent WT, *BOK*$^{-/-}$ mouse embryonic fibroblast (MEFs) cell lines were a generous gift of Dr. Samuel Katz at Yale School of Medicine, Pathology Department, New Haven, CT. Bak, Bax and *BOK*$^{-/-}$ and WT MEFs were grown in Dulbecco's modified Eagle medium (DMEM, catalog # 12800017, Invitrogen) supplemented with 10% heat-inactivated fetal bovine serum (FBS) (# 16000044, Thermo Fisher), 1% penicillin-streptomycin (PS) (# 15140122**,** Invitrogen) and 1% non-essential amino-acids (# M7145, Sigma). MDCK (Madin-Darby Canine Kidney Epithelial Cells), A549 (Adenocarcinomic human alveolar basal epithelial cells), and Vero cells (Kidney epithelial cells from African green monkey) were purchased from the American Type Culture Collection (ATCC). Bv2 cells were a gift from Dr. Mohammad Javdan at Queensborough Community College, Biology Department, Queens, NY. MDCK and Bv2 cells were grown in DMEM supplemented with 10% FBS and 1% PS. A549 cells were maintained in F-12K Medium (Kaighn's Modification of Ham's F-12 Medium, # 21127022, Thermo Fisher**)** supplemented with 10% FBS and 1% PS. Vero cells were grown in Eagle's Minimum Essential Medium (EMEM) (# M0894, Sigma) supplemented with 10% FBS and 1% PS. All cell lines were incubated at 37° C under a humidified 5%CO_2 95% air atmosphere.

WT and *BOK*$^{-/-}$ MEFs were seeded at 2×10^5 cells per plate and allowed them to attach overnight in maintenance media. Cells were washed with 1X phosphate-buffered saline (PBS) and when appropriate staurosporine (STS) (# 62996-74-1, Sigma) was

dissolved in maintenance media at 5mM final concentration, and the cells were further incubated for 24h.

Macrophage extraction and cell culture

Swiss Webster male and female mice were injected 1 ml of 5% thioglycollate media (# 0190C81, Thomas Scientific) directly into the intraperitoneal cavity with a 1cc BD insulin syringe outfitted with a 28G, 1/2inch needle. The treated mice were sacrificed by CO_2 and cervical dislocation on the 4^{th} day following injection. One mouse at a time was placed on clean sheet of aluminum foil and sprayed with 70% ethanol. A small incision was made in the center of the abdomen exposing the peritoneal cavity. Using a 5 ml syringe, 10 ml of 1X sterile Phosphate Buffered Saline (PBS) was injected into the peritoneal cavity, then the peritoneal cavity was massaged several times to increase the yield of macrophages. Using a 22 G 1inch needle 5 ml of fluid from the peritoneal cavity was extracted and transferred to a 15 ml conical tube. This step was repeated 3 times to extract all the cells. In total 20 ml of fluid was collected and spun at 1500g for 10 minutes. The supernatant was discarded, and the pellet was resuspended in ice cold sterile distilled water to lyse red blood cells. The cells were spun again at 1500g for 10 minutes. The supernatant was discarded, and the pellet was resuspended in RPMI medium 1640 (catalog no. 21870076, Gibco) supplemented with 20% FBS, 1% PS. The cells were seeded at 4×10^5 into 35 mm plates with 22 mm^2 sterile glass coverslips (# 2870-22, Corning). Cells were incubated at 37° C in a humidified atmosphere with 5% CO_2.

Isolation, culture and titration of ZIKV

ZIKV-MR766 (ATCC® VR-84™) was cultured in Vero Cells for 3 days at 37° C and a humidified 5% CO_2 atmosphere. Vero cells were seeded at 3×10^6 cells in 75T flasks (# 156499, Laboratory Disposable Products) and allowed to attach overnight. Cells were infected at multiplicity of infection (MOI) of 0.1 for 2 hours, then cells were covered with DMEM with 2% FBS. After 3 days, supernatant was collected and cleared by centrifugation at 2,000 rpm at 4° C for 10 min. The supernatant was collected, aliquoted and stored at −80° C. Virus titer was determined by the traditional plaque assay. Monolayers of Vero cells were incubated in 12 well plates overnight in DMEM supplemented with 10% FBS and 1% penicillin. The cultures were then infected with 10-fold serial dilutions of virus suspension for 2 h at 37° C. Cells were then covered with the agar overlay, containing 50% low melting point agar (# V2111, Promega), 40% 2X DMEM and 10% FBS. The agar overlay was allowed to solidify at room temperature (RT) and the cells were incubated for 5 days at 37° C to promote plaque development. Immediately prior to plaque analysis, cells were fixed with 4% formaldehyde (# F8775, Sigma) for 20 minutes, then the solidified agar was removed, and cells were washed with 1X Phosphate Buffered Saline (1XPBS) and stained with a 1% crystal violet solution (# C0775, Sigma) for 10 minutes. Plaques were counted, and the virus titer was expressed as PFU/ml.

Influenza A viral growth and titer determination

Influenza A/WSN/33 virus was cultured in 10-day-old specific-pathogen-free embryonated chicken eggs (# 10100326, Charles River), for 2 days at 35° C. Infected egg

albumen was collected and cleared by centrifugation at 1,000 rpm for 10 min. The supernatant was collected, aliquoted and stored at −80°C. Virus titer was determined by plaque assay. Monolayers of MDCK cells were incubated overnight in DMEM containing 10% FBS and 1% PS, followed by infection with 10-fold serial dilutions of virus suspension for 1 h at RT. Virus was removed and cells were then covered with warmed DMEM containing 0.1% DEAE-dextran and 1% purified agar. This agar medium was allowed to solidify at RT and the plates were incubated for 2 days at 37° C to promote plaque development. Immediately prior to plaque analysis, the solidified agar was removed, and cells were fixed (4% formaldehyde) and stained with a 1% crystal violet solution. Plaques were counted, and the virus titer was expressed as PFU/ml.

Quantification of cell death

The effect of virus-induced cell death in the different cells lines was assessed by using the trypan blue exclusion assay. Exponentially growing cells were seeded at 2×10^4 cells per plate and allowed them to attach overnight before ZIKV infection. Cells were infected at MOI of 5 and the uninfected cells (controls) were incubated with viral dilution media (VDM) for 2 hours at 37° C under a humidified 5% CO_2 atmosphere and then DMEM containing 2%FBS was added. Cell were incubated at 37° C until collection. For influenza virus, cells were infected at MOI of 5 and the uninfected cells were incubated with VDM. Both conditions were incubated for 1 hour at 37° C; then the virus solution or VMD was removed and cells were washed with 1XPBS to remove the unattached virus and covered with DMEM containing 10% FBS and 1% PS. Infected and uninfected cells were detached from culture plates by trypsin digestion. Samples were

mixed 1:1 with 0.4% trypan blue (catalog no 15250061, Thermo Fisher Scientific) and incubated at RT for 5 min. Trypan blue is taken up by dead cells and excluded from living cells by their intact cell membranes. Cells were counted by use of a hemocytometer. In all cases, percent of cell viability was calculated as the ratio of live cells to the total number of cells.

MTT (3-(4, 5-dimethylthiazolyl-2)-2, 5-diphenyltetrazolium bromide) (MTT) assay

The MTT assay was used to measure mitochondrial respiration and indirectly cell proliferation. MTT (# M5655, Sigma) stock solution was prepared by solubilizing 5 mg/ml MTT in RPMI-1640 without phenol red and was then filtered through a 0.2 μM filter. MTT working solution was 1:10 in acetone or 0.5mg/ml MTT. *BOK*$^{-/-}$, WT MEFs and female and male macrophages were seeded at 1.5×10^5 cells per plate and allowed to attach overnight before viral infection. After 24h infection, cells were washed with warm 1XBS; MTT was added into wells being assayed; and cells were incubated at 37° C for 3 hours. Then the MTT solution was removed and the converted dye was solubilized with DMSO and placed on a plate shaker to make sure the converted dye dissolved completely. The solubilized solution was then transferred into a 1.5 mL Eppendorf tube and centrifuged at 13,000 RPM for 2 minutes. The supernatant was then transferred into a 96 well plate with black wells and a clear bottom and absorbance was measured at a wavelength of 570 nm with background subtraction at 650 nm.

Immunofluorescence

MDCK, A549, Vero, Bv2, BAK, BAX, *BOK*$^{-/-}$, WT MEFs and male and female macrophages were grown on glass coverslips to 70% confluence and incubated for 24h, followed by ZIKV infection at MOI of 5. Cells were washed twice with 1XPBS, fixed with 4% formaldehyde and permeabilized with 0.2% Triton X-100 (catalog no X100, Sigma) in 1X PBS for 15 min at 37° C, then cells were washed with 1X PBS for 5 minutes each. All antibodies were diluted in 1XPBS containing 1% BSA-0.1% Triton X-100. Cells were treated with 1% BSA (# A2153, Sigma) -0.1% Triton X-100 in 1X PBS for 1h before addition of antibodies. Cells were incubated overnight at 4° C with viral E protein mouse monoclonal primary antibody (1:10; Hybridoma cells), or cleaved caspase 3 monoclonal antibody (1:400, # 9664, Cell Signaling). Cells were washed 3 times with 1X PBS for 5 minutes. Cells were incubated with Alexa Fluor 488-conjugated goat anti-mouse IgG secondary antibody (1:1000; # A-21202, Molecular Probes) for 1 hour at room temperature. They were then washed with 1X PBS for 5 minutes and then stained with DAPI (1 mM) (# ab228549, ABCAM) for 8 minutes. Cells were washed twice with 1x PBS, mounted and embedded in Gel Mount (# F4680, Sigma) and observed by fluorescence microscopy.

Quantitative RT-PCR

Cells lines were infected and treated as described above. Total mRNA was isolated with the RNeasy Mini Kit (# GE25-0500-71, Sigma) according to the manufacturer's protocol. Then 100ng of RNA was amplified by using the Power SYBR™ Green RNA-to-Ct™ 1-Step Kit (catalog no. 4391178, Thermo Fisher) and the

expressions ZIKV gene NS1 and tubulin were determined using the following primers: NS1 gene forward primer TACACCC AGTCACAATAGGAGAGTG and reverse primer CCATGCATTCATTGTCACACTTGTGG and tubulin was analyzed with the forward primer AGGATTCGCAAGCTG GCTG and the reverse primer TAATCCACAGAGAGCCGCTCC. Relative viral RNA was compared with RNA from mock-infected cells. PCRs for each sample were done in triplicate for the target gene and tubulin.

Results

ZIKV infection and cell tropism

To determine the cell populations most susceptible to ZIKV infection, we investigated the infectivity of ZIKV in Vero, MDCK and A549 cells. All the cell lines were infected with the African (MR766) strain of ZIKV at MOI of 5, and then infectivity was detected by measuring the expression of ZIKV envelope protein by immunofluorescence after 24 hours post-infection (hpi) **(Figure 1A).** Envelope protein was detected in MDCK, Vero and A549 cells; although the expression levels, representing infectivity, were significantly high and different among MDCK, Vero and A459 cells (about 80% in MDCK, 100% in Vero and 90% in A549 cells) **(Figure 1B).** The extensive tropism results in ZIKV detection in different cell lines from different organisms.

ZIKV kills some cell lines

To determine the cell populations most susceptible to ZIKV infection, we infected Vero, MDCK and A549 cells for 24hpi and cell viability was measured by trypan blue. ZIKV kills Vero cells **(Figure 2B);** however, ZIKV did not kill MDCK or A549 cells even though the percentage of infectivity is very high **(Figure 1B)**. ZIKV killed 15% of Vero cells compared with uninfected cells by activating apoptotic rather than autophagic pathways **(Figure 2B).**

Microglial cells are one of the main targets of ZIKV in the developing brain (42, 46, 47). Microglia are mononuclear phagocytes that play an important role in neuronal development, as well as in the homeostasis of the central nervous system; they have a

marked impact on normal brain functioning and maintenance of tissue integrity (47). Therefore, we also studied the effects of ZIKV in the microglia Bv2 cells. We analyzed viral infection by immunofluorescence (Envelope protein) and RT-PCR for viral RNA (NS1 gene). ZIKV can infect Bv2 cells. The infected Bv2 cells expressed the viral E protein as well as the viral RNA (NS1 gene) compared with the uninfected cells **(Figure 3A-B).** We also investigated whether ZIKV kills Bv2 cells by measuring cell viability. Interestingly, we found that ZIKV infection did not kill a significant number of Bv2 cells after 24 hpi compared with the uninfected cells **(Figure 3C)**. We also asked whether infection altered their phagocytosis. Bv2 cells were infected for 2 hours followed by addition of microspheres as well as media. After 24 hpi, we counted the microspheres that were phagocytosed by the uninfected and infected Bv2. The difference in percentage of cells that phagocytosed was insignificant. (**Figure 3D).** These data indicate that although ZIKV infected Bv2 cell, ZIKV did not kill them or alter phagocytosis function after 24hpi.

ZIKV infects primary male and female macrophages in a sex dimorphic manner

As most of these cells are not primary, we asked whether the effect of ZIKV would differ in primary cells since in many ways they are closer to the *in vivo* target of the virus. Since male and female mouse macrophages (which phagocytose pathogens and then undergo apoptosis, limiting spread of infection) differ in their ability to carry out phagocytosis (data not published), we asked whether primary macrophages extracted from male and female mice differed in their response to ZIKV. First, we examined whether ZIKV preferentially infects in a sex dimorphic manner. Primary macrophages

harvested from male and female mice were incubated in culture medium followed by ZIKV infection for 24h at MOI of 5. Infectivity was confirmed by immunofluorescence for the viral E protein and by RT-PCR for viral RNA. Both infected male and female cells showed the expression of the viral E protein **(Figure 4A**) and also the expression of the viral RNA after 24 hpi. Interestingly, the viral RNA was 4 times higher in the infected-female compared with the infected-male macrophages **(Figure 4B).** We also tested the ability of female and male macrophages to produce viral progeny *in vitro* by determining viral titers in the supernatants of the ZIKV-infected cells using a standard plaque assay. The infected female macrophages have a higher active viral replication compared with the infected male macrophages. ZIKV-infected female produced 29% higher titers compared with the ZIKV-male macrophages. Overall, these results suggested that female macrophages are more easily infected and more readily produce viral progeny compared with male macrophages **(Figure 4C).**

Since female macrophages produced more virus compared with males, we asked whether ZIKV kills infected female and male macrophages. Male and female macrophages were infected with ZIKV for 24h at MOI of 5 followed by analysis of cell viability by trypan blue. ZIKV killed 10% of infected-female macrophages but did not kill infected male macrophages compared with the uninfected macrophages (**Figure 5A).** To corroborate these results, we performed MTT assay to measure cellular respiration as an indirect method of cell proliferation. Cellular respiration did not change in the ZIKV-female macrophages and ZIKV-male macrophages compared with the uninfected female and macrophages, respectively **(Figure 5B).**

Since the main function of the macrophages is to phagocytose pathogens to limit viral infection, we asked whether ZIKV altered the ability of the macrophages to phagocytose. Male and female macrophages were infected with ZIKV for 2 h and then microspheres were added (5beads/per cell) as well as media. The number of beads that uninfected and infected-macrophages phagocytosed was counted 24 hpi. The differences between infected-female macrophages that phagocytosed beads compared to uninfected female macrophages and between infected male and female cells were insignificant **(Figure 5C).**

Overall, these results suggested that female and male macrophages can be infected by ZIKV (measured by IF and RT-PCR), but the female macrophages are better cells to produce higher amounts of virus compared with the male macrophages. Furthermore, ZIKV does not alter their phagocytosis. We have not resolved the generality of this observation, as our cell lines come from diverse sources (MDCK: canine kidney, [female]; A549: human adenocarcinoma, [male]; Vero: monkey kidney, [sex unknown]; Bv2: mouse microglia, [sex unknown]; MEF (knockout cells) mouse embryonic fibroblasts [sex unknown].

The Bcl-2 family proteins regulates cell death

The pathogenesis of viral infections involves dynamic interactions between viruses and hosts, which can result in different outcomes including cell killing and elimination of the virus (26, 27). Viruses have evolved multiple strategies to subvert host cell apoptosis in response to infection. The inhibition of apoptosis can alter the course of virus replication and propagation of viruses (13, 33). Therefore, we asked

whether the inhibition of the pro-apoptotic Bcl-2 proteins, especially BAX and BAK, enhanced the replication of ZIKV. To test whether the genetic inhibition of the pro-apoptotic proteins protect cell from cell killing and production of ZIKV. The WT, $BAK^{-/-}$ and $BAX^{-/-}$ MEFs were infected with ZIKV for 24 hours at MOI of 5 followed by immunofluorescence for the envelope protein to confirm infectivity. The WT, BAK and BAX MEFs cells are infected by ZIKV (green signal, **Figure 6A**). The envelope protein was detected in WT, $BAK^{-/-}$ and $BAX^{-/-}$ MEFs although the expression levels, representing infectivity, were significantly different among the MEFs. Only 28% of the WT MEFs were infected compared with the 50% and 70% of $BAK^{-/-}$ and $BAX^{-/-}$ MEFs **(Figure 6B).** In fact, percent of BAX and BAK knockout cells infected were as high as in MDCK cells **(Figure 1A).**

We also asked whether the loss of BAX and BAK protects the cells from apoptosis. BAX, BAK and WT MEF's cells were infected with ZIKV and we measured the cell viability by the trypan blue assay. The difference in cell death between infected knockout cells compared with the uninfected knockout cells and infected WT cells was not significant and in all cases was less than 5% **(Figure 6C).**

The role of the pro-apoptotic Bcl-2 family member (*BOK*) during ZIKV infection

ZIKV induces ER stress activating the PERK-mediated UPR pathway, which is potentially linked to high cell death and is perhaps the predominant driver of ZIKV-induced microcephaly (46). Therefore, we examined the relevance of the PERK pathway to viral propagation. Vero cells were pre-treated with salubrinal (a chemical inhibitor that

de-phosphorylates eIF2α, inhibiting the PERK pathway (49)) for 1h and then infected with ZIKV for 24 h. The viral RNA was measured by RT-PCR and also the virus progeny was measured by the traditional plaque assay. In both cases, we found that the inhibition of PERK pathway reduced the production of ZIKV. The infected cells that were pre-treated with salubrinal produced 50% less virus compared with the infected cells alone (data not shown).

We investigated the role of *BOK* during ZIKV infection. *BOK* is a pro-apoptotic protein that induces apoptosis in response to ER stress by activating the PERK pathway (49). Therefore, we decided to investigate the role of *BOK* in infected cells. WT and *BOK*$^{-/-}$ MEFs' cells were infected with ZIKV for 24h at MOI of 5. Cell death in response to ZIKV infection was assessed by the trypan blue exclusion assay. Unlike Vero cells and female macrophages, ZIKV was not lethal to MEF regardless of the status of BOK pathway. The amounts of cell death in WT and *BOK*$^{-/-}$ were insignificantly different from control at 24hpi **(Figure 7A),** although BOK$^{-/-}$ cells were more resistant to both STS and flu than WT**.** Also, there was no cytopathic effect as defined by rounding of the cells in the infected or uninfected cells after 24hpi (data not shown). To corroborate the finding that BOK induced apoptosis in response to ER stress, we infected the WT and *BOK*$^{-/-}$ cells with influenza virus (IVA) or treated them with protein kinase inhibitor staurosporine (STS) to induce apoptosis. WT and *BOK*$^{-/-}$ MEFs were both readily killed by combined exposure to STS and IVA. Cell viability decreased 90% and 95% in the WT cells after STS or IAV infection and 60% and 50% in the *BOK*$^{-/-}$ cells, respectively **(Figure 7A).** Cytopathic effect, rounding of the previously elongated cells, was also visible at 24h. In both cases, WT and *BOK*$^{-/-}$ cells were rounded and smaller. Cells

infected with ZIKV but with no STS did not present any further cytopathic effect after infection (data not shown). Apoptosis was analyzed by the detection of cleavage of caspase 3 by immunofluorescence. Cleavage of caspase 3 was detected in the STS and IVA MEFs (green signals) but not in the WT and *BOK*$^{-/-}$ cells infected ZIKV MEF but not exposed to STS **(Figure 7B).**

BOK$^{-/-}$ is required for expression of viral RNA and production of virus

We determined that ZIKV did not kill WT and *BOK*$^{-/-}$ cells but we did not measure production of ZIKV. We hypothesized that the loss of *BOK*$^{-/-}$ would nevertheless affect the production of ZIKV. To test our hypothesis, we infected WT and *BOK*$^{-/-}$ cells and analyzed the amount of viral RNA (by RT- qPCR) at different times, viral proteins (by immunofluorescence) and the virus progeny (traditional plaque assay). The percentage of infectivity was calculated by counting the cells that were positive for E protein (green) over the total number of cells. The % infectivity was 25% higher in the *BOK*$^{-/-}$ cells compared with WT **(Figure 8A-B).** We also detected more intracellular copies of virus RNA with RT-PCR compared to number of virus secreted in the supernatant, as detected with plaque assay. Thus, the numbers of active viral progeny released in the supernatant might not correlate with the amount of intracellular viral RNA. Overall, these results indicated that *BOK* is important for maturation of the virus **(Figure 8C-D).**

Discussion

ZIKV pathogenesis exhibits broad cell tropism and persistence. Our data indicates that ZIKV infects different cell lines that come from diverse sources (MDCK: canine kidney; A549: human adenocarcinoma, Vero: monkey kidney, Bv2: mouse microglia, MEF (knockout cells) mouse embryonic fibroblasts) and does not prefer a specific cell line. The expression of the viral E protein is strong in all the cells lines tested. Next, the extent to which ZIKV induces cell death was analyzed by trypan blue exclusion assay. Interestingly, we found that ZIKV induces 20% cell death in Vero by activating apoptotic pathways. In contrast, ZIKV did not significantly kill other cell lines such as MDCK, A549 and Bv2 cells, as measured at 24 hpi. We hypothesized that ZIKV could take over autophagy as an alternative pathway, which might improve ZIKV replication. There is evidence suggesting that autophagy pathway can be modulated by ZIKV infection. ZIKV was shown to induce autophagy in skin fibroblasts (50) and human fetal neural stem cells (51) and this was associated with enhanced replication (53).

We also investigated whether ZIKV infection is sex dimorphic. ZIKV proved to be able to infect both male and female macrophages, but the female macrophages produce more virus compared with the male macrophages. Even though female produce more virus, neither their phagocytosis nor their viability is altered. Future studies on sex dimorphism in macrophages during ZIKV infection will give us insight on the underlying mechanisms and key factors responsible for sex differences in viral production.

Viruses have evolved ways to prevent premature death of infected cells, thereby facilitating virus replication and production of progeny. The percentage of infectivity is higher in the Bax and Bak knockout MEFs compared with the WT, suggesting that apoptosis is an organismal defense against virus. It has been reported that ZIKV replication machinery is established at the ER membrane and excessive synthesis of viral protein may lead to ER stress (19,53). UPR is activated to mitigate unfolded protein load by pro-survival mechanisms such as ER membrane expansion, decreased influx of proteins into ER or induction of transcription of key components of protein folding. UPR can also up-regulate autophagy thus increasing ZIKV replication and preventing neurogenesis (52). If the ER stress is prolonged, apoptosis can be induced (53). Therefore, we examined the role of BOK, the new pro-apoptotic member of Bcl-2 protein family, which regulates apoptosis in response to ER stress (50). To understand if *BOK* is activated during ZIKV infection, we used MEFs that lack BOK. In cells lacking *BOK*, the rates of apoptosis (demonstrated by trypan blue exclusion) are not significantly different compared to those of the infected WT. We hypothesized that, nevertheless, *BOK* is important for viral translation. We measured the amount of viral RNA and also the viral progeny released at different times. We found that the viral RNA was higher in the *BOK*$^{-/-}$ cells compared with WT. However, WT released more virus particles than *BOK*$^{-/-}$ cells. In spite of infectivity of WT and *BOK*$^{-/-}$ (~25% and 50% with MOI of 5), we detected relatively few virus (in the range of 100-10,000 PFU/mL) suggesting that the mouse embryonic fibroblasts are efficiently infected but with limited capacity to produce viral progeny and that they are less capable of producing virus when they lack BOK. These results indicated that ZIKV requires BOK to replicate.

ZIKV infection still constitutes an ongoing challenge that requires strict surveillance and attention. It is the necessity to unravel ZIKV biology and the mechanisms involved in virus–host cell interactions to have a better understanding of these processes to develop new strategies for designing therapeutics and vaccines against ZIKV

References

1. Alfano, Christian et al. 2019. The Unfolded Protein Response: A Key Player in Zika Virus-Associated Congenital Microcephaly. Front Cell Neurosci. **13**: 94 [PubMed].

2. Hastings, Andrew K et al. 2019. Loss of the TAM Receptor Axl Ameliorates Severe Zika Virus Pathogenesis and Reduces Apoptosis in Microglia. Science. **13**: 339-350. [PubMed].

3. Lee, Ying-Ray et al. 2018. Dengue virus-induced ER stress is required for autophagy activation, viral replication, and pathogenesis both in vitro and in vivo. Sci Rep. **8,1**: 489. [PubMed].

4. Muñoz, Laura S et al. 2017. Neurological Implications of Zika Virus Infection in Adults. J Infect Dis. **216**: S897–S905 [PubMed].

5. Pihán, Philippe et al. 2017. BCL-2 family: integrating stress responses at the ER to control cell demise. Cell Death Differ. **24(9):**1478–1487 [PubMed].

6. Chen, Qi et al. 2018. Treatment of Human Glioblastoma with a Live Attenuated Zika Virus Vaccine Candidate. mBio. **9**:5 [PubMed].

7. Datan, E et al. 2015. Dengue-induced autophagy, virus replication and protection from cell death require ER stress (PERK) pathway activation. Cell Death Dis. **7,3**: e2127 [PubMed].

8. Gaston, Bonenfant et al. 2019. Zika Virus Subverts Stress Granules to Promote and Restrict Viral Gene Expression. J Virol [PubMed].

9. Kuno, G et al. 1998. Phylogeny of the genus Flavivirus. J Virol. **72,1**: 73-83 [PubMed].

10. Miner, Jonathan J, and Michael S Diamond. 2017. Zika Virus Pathogenesis and Tissue Tropism. Cell Host Microbe. **21,2**: 134-142[PubMed].

11. Valadão, Ana L C et al. 2016. Interplay between Inflammation and Cellular Stress Triggered by Flaviviridae Viruses. Front Microbiol. **7**:1233 [PubMed].

12. Dick G. W., Kitchen S. F., Haddow A. J. 1952. Zika virus. I. Isolations and serological specificity. Trans. R. Soc. Trop. Med. Hyg. **46,5**: 509–520 [PubMed].

13. Gorshkov, Kirill et al. 2018. Zika Virus: Origins, Pathological Action, and Treatment Strategies. Front Microbiol. **9:** 3252 [PubMed].

14. Hastings, Andrew K, and Erol Fikrig. 2017. Zika Virus and Sexual Transmission: A New Route of Transmission for Mosquito-borne Flaviviruses. Yale J Biol Med. **90,2**: 325-330 [PubMed].
15. Hussain, Azhar et al. 2018. A Comprehensive Review of the Manifestations and Pathogenesis of Zika Virus in Neonates and Adults. Cureus. **10,9**: e3290. [PubMed].

16. Miner, Jonathan J, and Michael S Diamond. 2017. Zika Virus Pathogenesis and Tissue Tropism. Cell host microbe. **21,2**: 134-142 [PubMed].

17. White, Martyn K et al. 2016. Zika virus: An emergent neuropathological agent. Ann Neurol. **80,4**: 479-489 [PubMed].

18. Depoux, Anneliese et al. 2017. A multi-faceted pandemic: a review of the state of knowledge on the Zika virus. Public health Rev. **39**:10 [PubMed].

19. Ojha, Chet Raj et al.2018. Complementary Mechanisms Potentially Involved in the Pathology of Zika Virus. Front Immunol. **9:**2340 [PubMed].

20. Panchaud, Alice et al. 2016. Emerging Role of Zika Virus in Adverse Fetal and Neonatal Outcomes. Clin Microbiol Rev. **29,3:** 659-694 [PubMed].

21. White, Martyn K et al. 2016. Zika virus: An emergent neuropathological agent. Ann Neurol. **80,4:** 479-489 [PubMed].

22. Liu, Jun et al. 2018. Zika Virus Envelope Protein induces G2/M Cell Cycle Arrest and Apoptosis via an Intrinsic Cell Death Signaling Pathway in Neuroendocrine PC12 Cells. Int J Biol Sci. **14,9:** 1099-1108 [PubMed].

23. Mukhopadyay, Suchetana. Kuhn J, Richard. Rossmann Michael J. 2018. A structural perspective of the flavivirus life cycle. Nat Rev Microbiol. **13,1:** 11-22 [PubMed].

24. Dai, Lianpan et al. 2016. Structures of the Zia Virus Envelope Protein and its Complex with a Flavivirus Broadly Protective Antibody. Cell Host Microbe. **19(5):**696-704 [PubMed].

25. Fuchs, Yaron. Steller, Hermann. 2011. Programmed Cell Death in Animal Development and Disease. Cell Press. **147, 4:** 742-758. [PubMed].
26. Kvansakul Marc. 2017. Viral Infection and Apoptosis. Viruses [PubMed].
27. Orzalli, Megan H, and Jonathan C Kagan. 2017. Apoptosis and Necroptosis as Host Defense Strategies to Prevent Viral Infection. Trends in Cell Bio. **27,11**: 800-809 [PubMed].

28. Ghosh Roy, Sounak et al. 2014. Regulation of cell survival and death during Flavivirus infections. World J Biol Chem. **5,2:** 93-105 [PubMed].

29. Okamoto, Toru et al. 2017. Regulation of Apoptosis during Flavivirus Infection. Viruses. **9,9**: 243 [PubMed].

30. Suzuki, Tatsuya et al. 2018. Infection with flaviviruses requires BCLXL for cell survival. PLoS Pathog. **14,9**: e1007299 [PubMed].

31. Green, Douglas R. Llambi, Fabien. 2015. Cell Death Signaling. Cold Spring Harb Perspect Biol. **7,12**: a006080 [PubMed].

32. Kvansakul, Marc et al. 2017. The Bcl-2 Family in Host-Virus Interactions. Viruses. **9,10:** 290 [PubMed].

33. Vicenzi, Elisa et al. 2018. Subverting the mechanism of cell death: flavivirus manipulation of host cell responses to infection. Biochemical Society Transactions. **46;3**: 609-617 [PubMed].

34. Opferman, Joseph T, and Anisha Kothari. 2017. Anti-apoptotic BCL-2 family members in development. Cell Death Differ. **25,1:**37–45 [PubMed].

35. Li, Mark Xiang, and Grant Dewson. 2015. Mitochondria and apoptosis: emerging concepts. F1000Prime Rep. **7:** 42 [PubMed].

36. Peña J, and Harris E. 2011. Dengue virus modulates the unfolded protein response in a time-dependent manner. J Biol Chem. **286,16**: 14226–14236 [PubMed].

37. Hetz, Claudio. 2012. The unfolded protein response: controlling cell fate decisions under ER stress and beyond. Nat Rev Mol Cell Biol.**13(2):**89-102 **[**PubMed].

38. Tan, Zhongyuan et al. 2018. ZIKV infection activates the IRE1-XBP1 and ATF6 pathways of unfolded protein response in neural cells. J Neuroinflammation**. 15,1:** 275 [PubMed].

39. Corazzari, Marco et al. 2017. Endoplasmic Reticulum Stress, Unfolded Protein Response, and Cancer Cell Fate. Front Oncol. **7:** 78 [PubMed].

40. Hou, Shangmei et al. 2017. Zika Virus Hijacks Stress Granule Proteins and Modulates the Host Stress Response. J Virol. **91,16**; e00474-17 [PubMed].

41. Sano, Renata, and John C Reed. 2013. ER stress-induced cell death mechanisms. Biochim Biophys Acta. **1833,12**: 3460-3470 [PubMed].

42. Ojha, Chet Raj et al. 2019. Toll-like receptor 3 regulates Zika virus infection and associated host inflammatory response in primary human astrocytes. PloS One.**14,2;** e0208543 [PubMed].

43. Fusakio, Michael E et al. 2016. Transcription factor ATF4 directs basal and stress-induced gene expression in the unfolded protein response and cholesterol metabolism in the liver. Mol Biol Cell. 27,9: 1536-1551 [PubMed].

44. Lee, Ying-Ray et al. 2018. Dengue virus-induced ER stress is required for autophagy activation, viral replication, and pathogenesis both in vitro and in vivo. Sci Rep. **8,1**: 489 [PubMed].

45. Schmitz, M Lienhard et al. 2018. The Crosstalk of Endoplasmic Reticulum (ER) Stress Pathways with NF-κB: Complex Mechanisms Relevant for Cancer, Inflammation and Infection. Biomedicines. **6,2** 58 [PubMed].

46. Gladwyn-Ng, Ivan et al. 2018. Stress-induced unfolded protein response contributes to Zika virus–associated microcephaly. Nat Neuroscie. 21: 63-71 [PubMed].

47. Ormel, Paul R. 2018. Microglia innately develop within cerebral organoids. Nat. **9,1**: 4167 [PubMed].

48. Boyce, Michael et al. 2005. A Selective Inhibitor of eIF2α Dephosphorylation Protects Cells from ER Stress. Science. **307**: 935-939 [PubMed].

49. Carpio, Marcos A et al. 2015. BCL-2 family member BOK promotes apoptosis in response to endoplasmic reticulum stress. Proc Natl Acad Sci U S A. **112,23:** 7201-7206 [PubMed].

50. Hamel, Rodolphe et al. 2015. Biology of ZIKV Virus Infection in Human Skin Cells. J. Virol. **89:**8880–8896 [PubMed].

51. Liang, Q et al. 2016. Zika virus NS4A and NS4B proteins deregulate Akt-mTOR signaling in human fetal neural stem cells to inhibit neurogenesis and induce autophagy. Cell Stem Cell. **19, 5:**663–671 [PubMed].

52. Gratton, R et al. 2019. Autophagy in Zika Virus Infection: A Possible Therapeutic Target to Counteract Viral Replication. Int J Mol Sci. **20,5:** 1048 [PubMed].

Figure 1: ZIKV infectivity in different cell lines

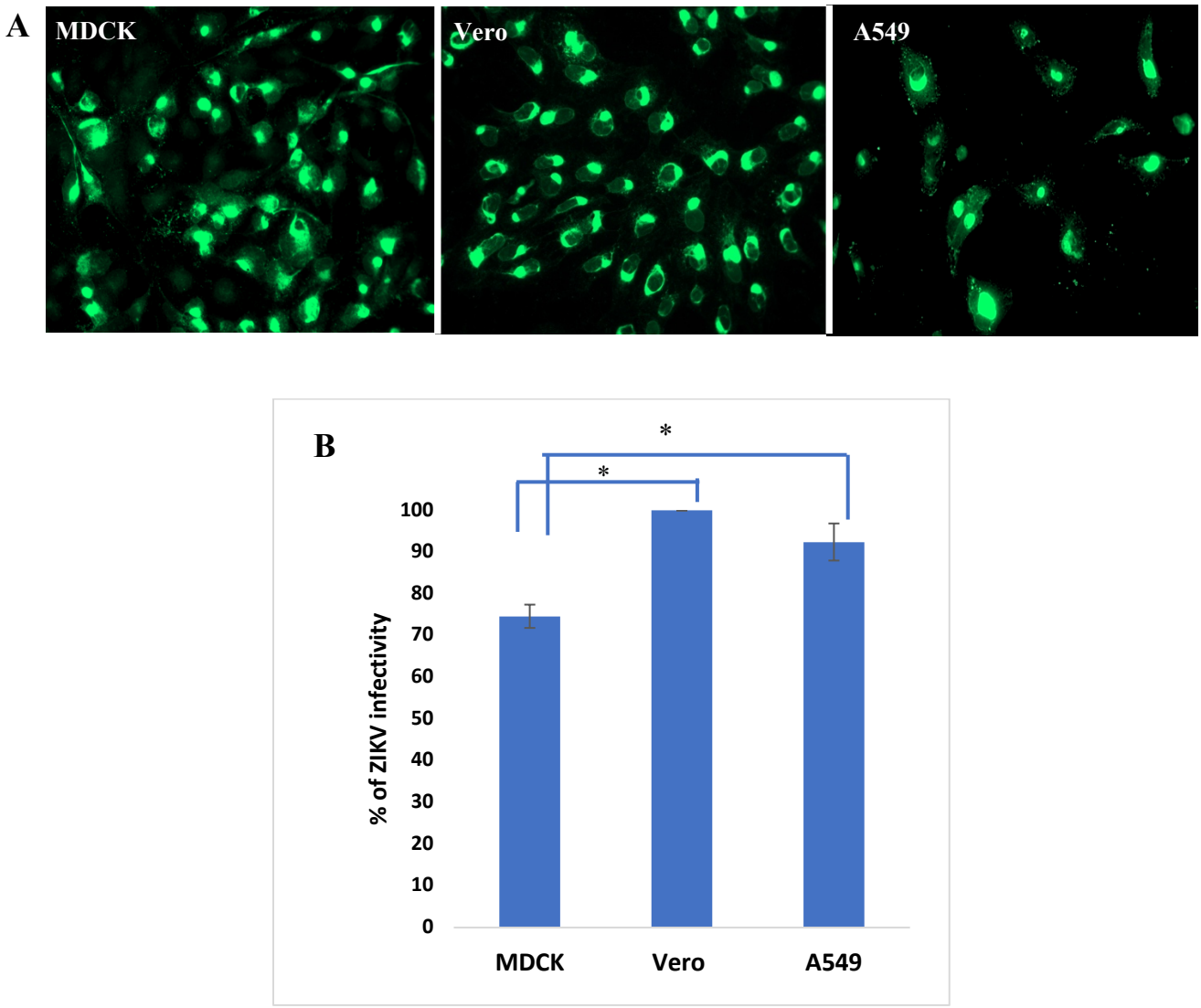

Figure 1: A. MDCK (Madin-Darby Canine Kidney Epithelial Cells), A549 (Adenocarcinoma human alveolar basal epithelial cells), and Vero cells (Kidney epithelial cells from African green monkey) were infected with ZIKV at MOI of 5 for 24h followed by the detection of the viral envelope protein (green) by immunofluorescence. **B.** Quantification of percentage of cell infectivity in the different

cell lines. The percentage was calculated by counting the cells that are positive for E protein (green) over the total number of cells. *p value <0.05.

Figure 2: Analysis of cell death by trypan blue assay

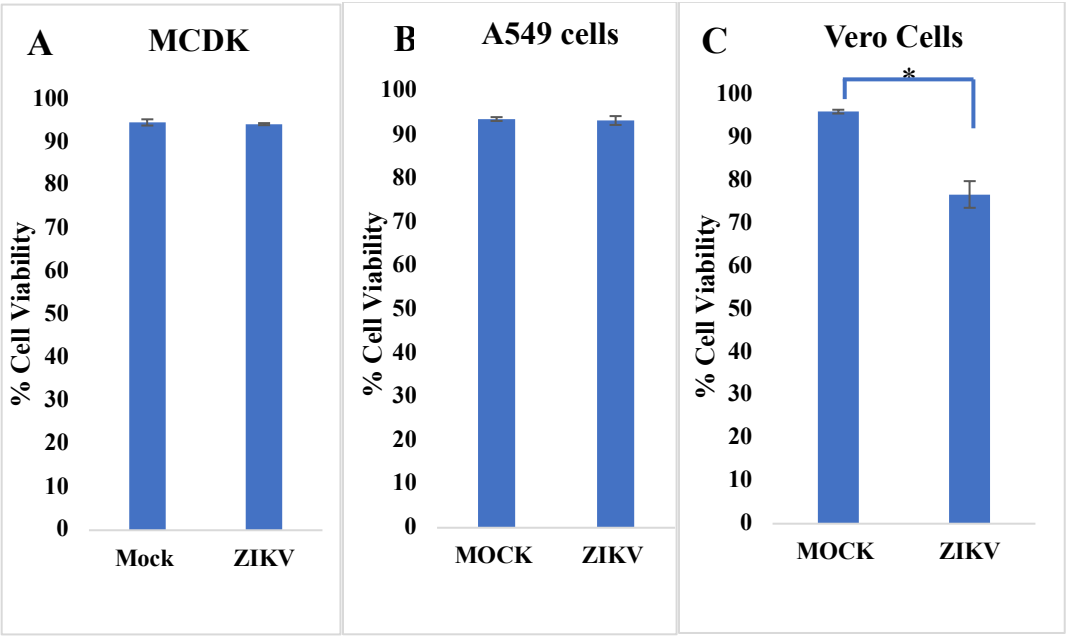

Figure 2: MDCK, A549 and Vero cells were infected with ZIKV at MOI of 5 for 24h. Uninfected cells were treated with viral dilution media (VDM) only. The amount of cell death was measured by trypan blue exclusion assay; only for the Vero cells did ZIKV kill more cells (15% more) than control. MDCK and A549 infected cells did not lose viability compared with the uninfected cells even though MDCK and A549 cells were highly infected (Figure 1B). *p value <0.05.

Figure 3: Analysis of ZIKV infection in Bv2 cells

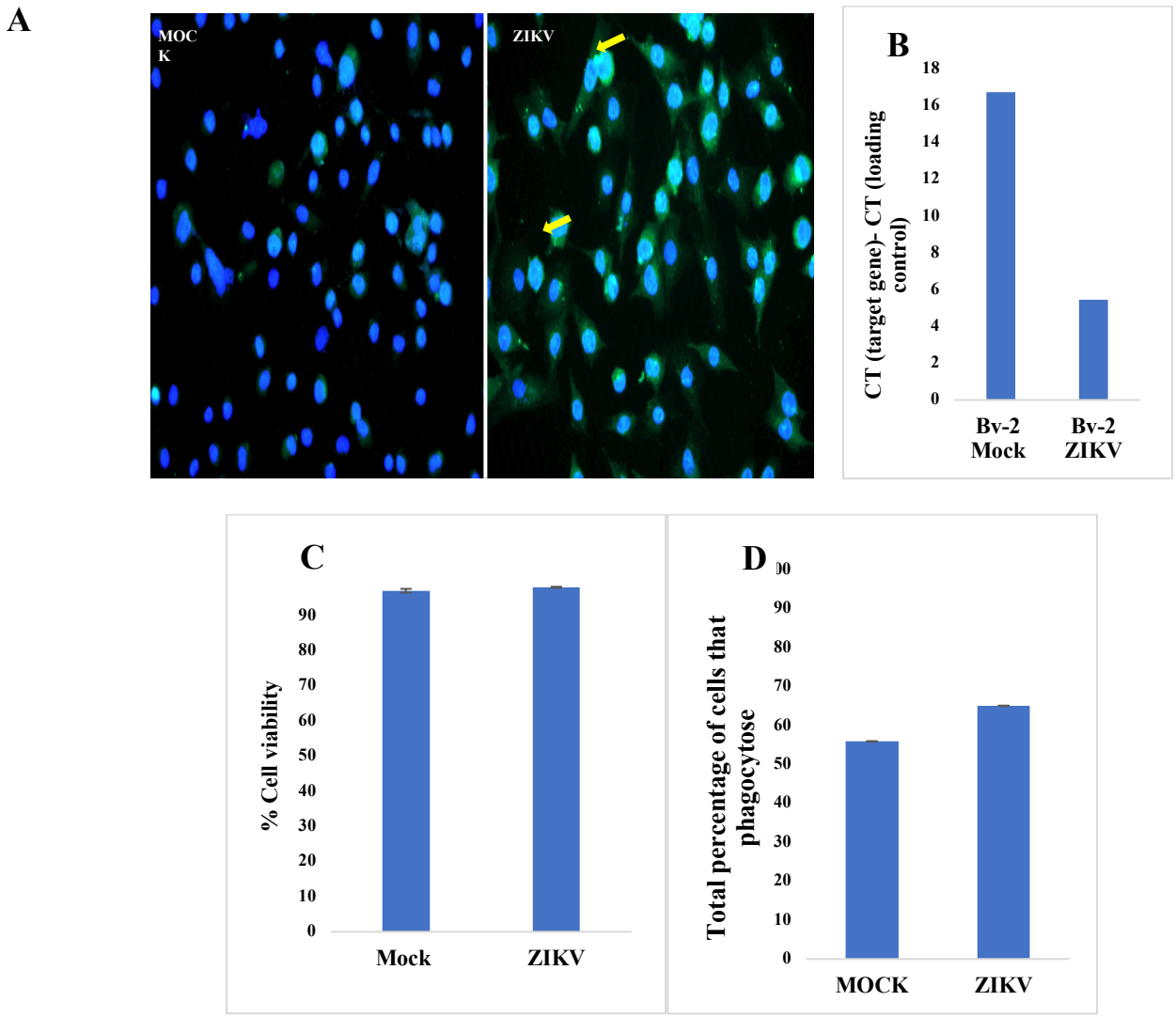

Figure 3: A-B. Infectivity of Bv2 cells was measured by immunofluorescence and RT-PCR. Bv2 cells were infected for 24h at MOI of 5 and uninfected cells were treated with VDM followed by immunofluorescence for E protein and RT-PCR for the viral NS1 gene. Bv2 infected cells showed viral envelope protein (green; yellow arrow) and the uninfected cells (mock) that did not show any signal of viral protein. DAPI was used for staining nuclei. The expression of the envelope protein was not strong compared with infectivity in MDCK, A549 and Vero (Figure 1A-C). The NS1 gene was present in the

infected cells but not in the control cells. **C.** Cell viability was measured by the trypan blue exclusion assay. ZIKV did not kill Bv2 infected compared with uninfected cells. **D.** Phagocytosis was measured in Bv2 infected cells compared with uninfected cells. Bv2 cells were infected with ZIKV for 2h or treated with VDM, then DMEM containing 2% FBS was added as well as microspheres (5 beads per cells) and they were kept for the 24h. Cells were mounted and embedded in gel and observed by fluorescence microscopy. The number of beads that each cell contained was counted and the percentage of cells that phagocytosed was quantified. The results showed that ZIKV did not affect the percentage of cells phagocytose or the number of beads per cell (not shown).

Figure 4: Infectivity of virus in female and male macrophages

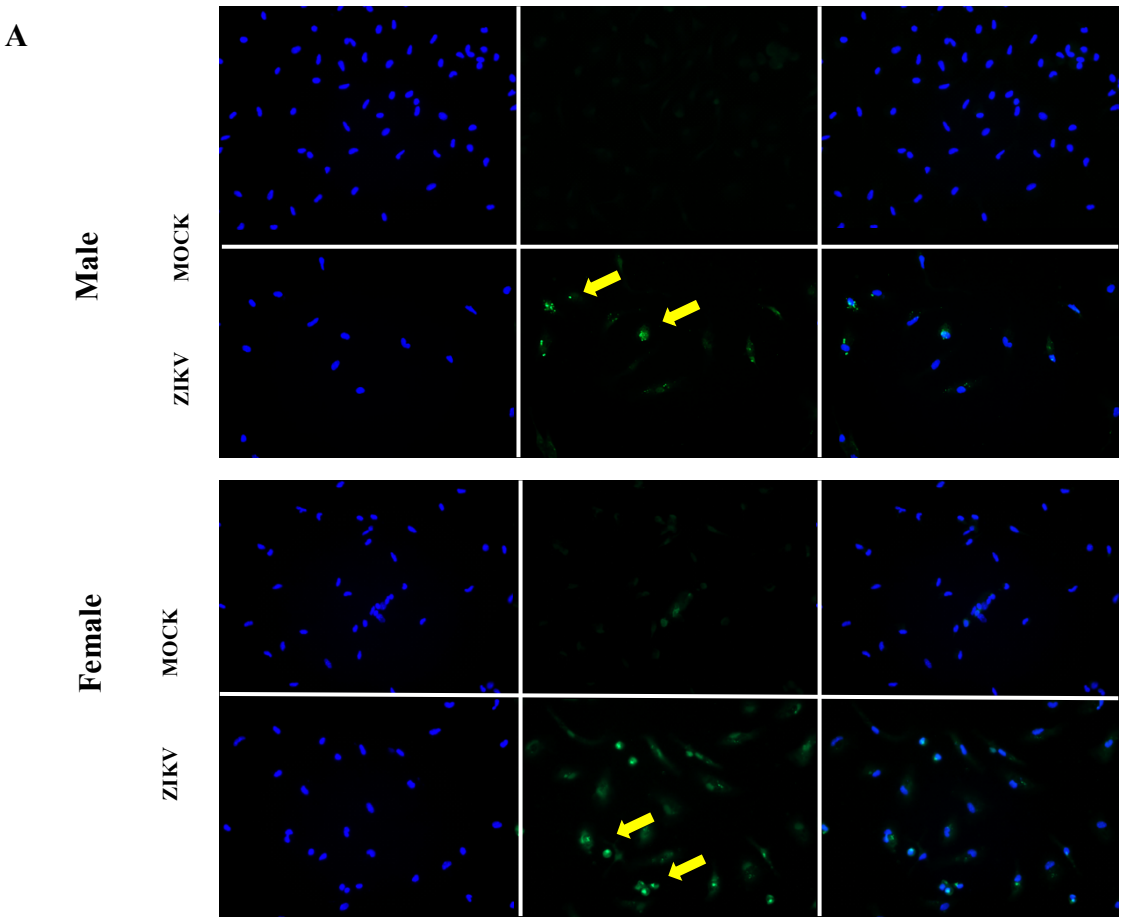

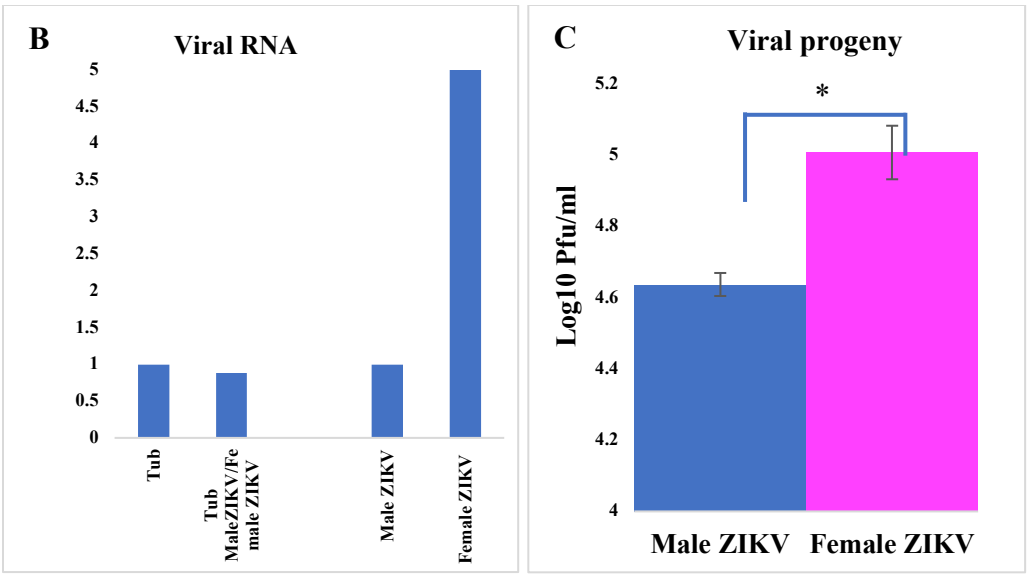

Figure 4: A. Primary male and female macrophages were infected with ZIKV at MOI of 5 for 24h. Infectivity was analyzed by IF for the viral E protein (green, yellow arrow). DAPI was used to stain nuclei. Both infected male and female macrophages expressed the viral envelope protein compared with the uninfected cells (mock; yellow arrows indicate infected male/female macrophages. **B.** Extracts of infected cells were used for RT-PCR to analyze viral RNA. Both infected male and female cells showed presence of viral RNA, but female had 5 times more viral RNA than the infected male cells. **C.** Viral reproduction was examined by the traditional plaque assay. The supernatants of infected male and female cells were collected and used to infect monolayers of Vero cells. Infected-female macrophages produced 55% more viral particles compared with the infected-male macrophages.

*p value <0.05.

Figure 5: Viability of infected macrophages

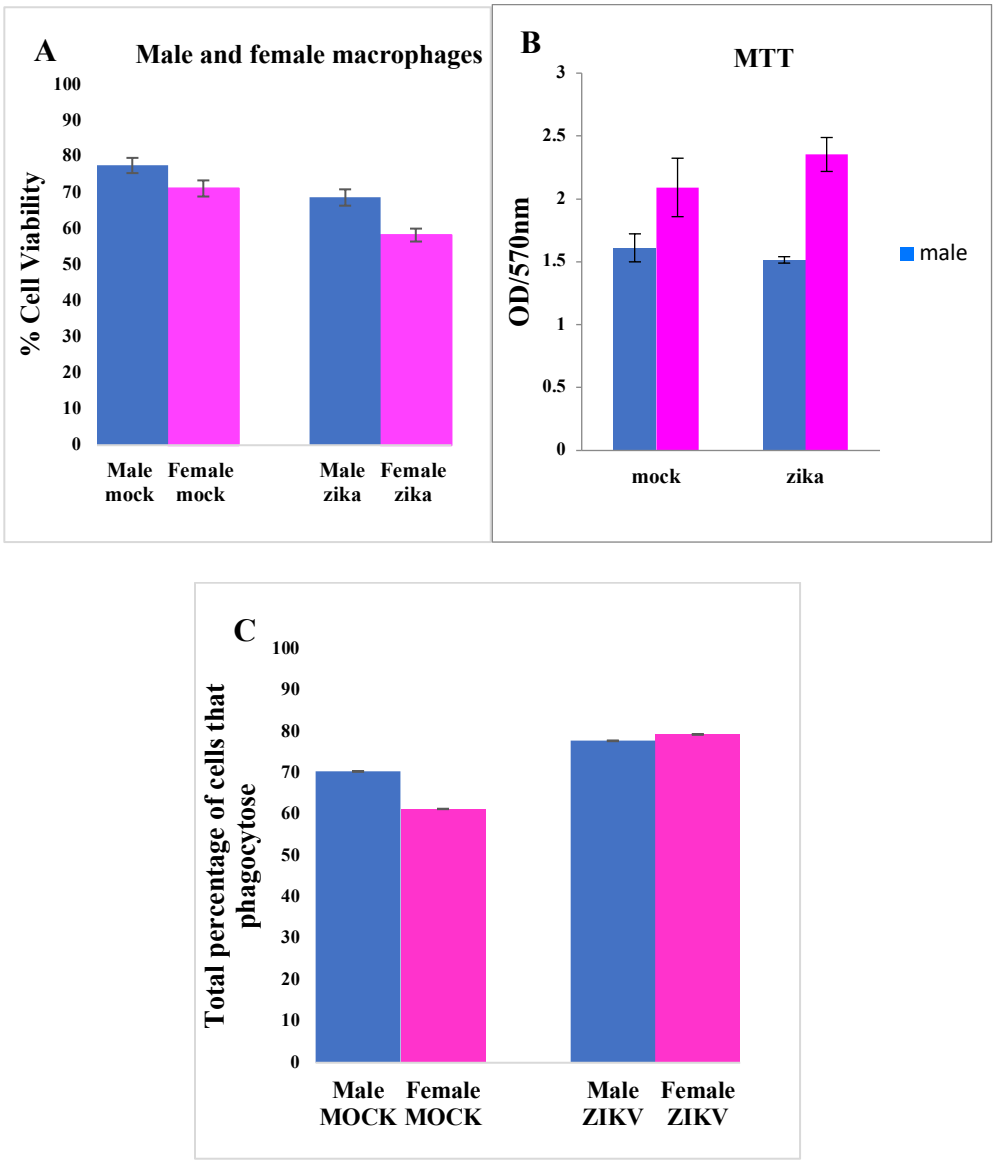

Figure 5: A. Male and female macrophages were infected for 24h and the uninfected cells were treated with viral dilution media (VDM) followed by the trypan blue exclusion assay. ZIKV killed 10% more female macrophages than male macrophages, but the difference was not significant. **B.** Cell respiration was measured by MTT assay as an indirect indicator of cell proliferation. Cell respiration was higher in the uninfected female macrophages compared with the uninfected male macrophages, and ZIKV does

not alter cellular reparation in either male or female macrophages compared with controls. **C.** Phagocytosis was measured in infected female and male macrophages that were infected with ZIKV for 2h; or they were treated with VDM and then medium was added with microspheres (5 beads/ per cells) and they were kept for the 24h. Cells were mounted and embedded in gel and observed by fluorescence microscopy. The number of beads that each cell was counted and the percentage of cells that phagocytosed was quantified. The results showed that ZIKV did not alter the phagocytosis ability of the infected and non-infected macrophages.

Figure 6: Infectivity of ZIKV in MEFs

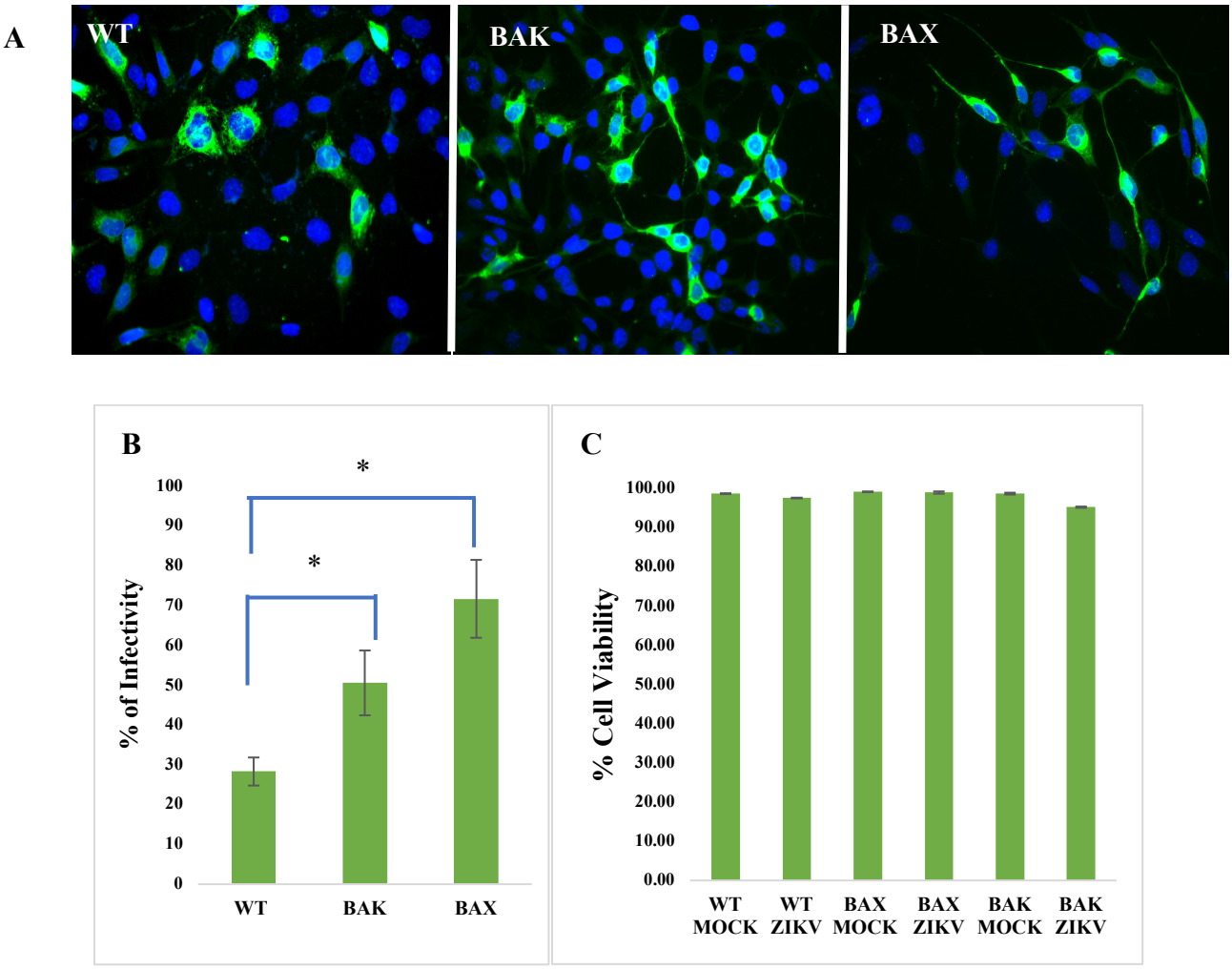

Figure: A. Wild type (WT), BAK$^{-/-}$ (BAK), BAX$^{-/-}$ (BAX) MEF's cells were infected with ZIKV at MOI of 5 followed by immunofluorescence after 24hpi. The E protein was expressed in the infected cells (green). DAPI was used for nuclei staining. **B.** Quantification of percentage of cell infectivity in the different cell lines. The percentage was calculated by counting the cells that are positive for E protein (green) over the total number of cells. Infected Bak$^{-/-}$ and Bax$^{-/-}$ cells showed higher infectivity (50% and 70% respectively) compared with the WT cells (20% infectivity). **C.** Cell viability was measured by the trypan blue exclusion assay. WT, BAX$^{-/-}$, BAK$^{-/-}$ MEF's cells were

infected at MOI of 5 for 24 and then cell viability was quantified. ZIKV did not kill the MEFs compared with the uninfected MEFs (mock). *p value <0.05.

Figure 7: Analysis of cell viability of ZIKV-infected *BOK*$^{-/-}$ MEFs.

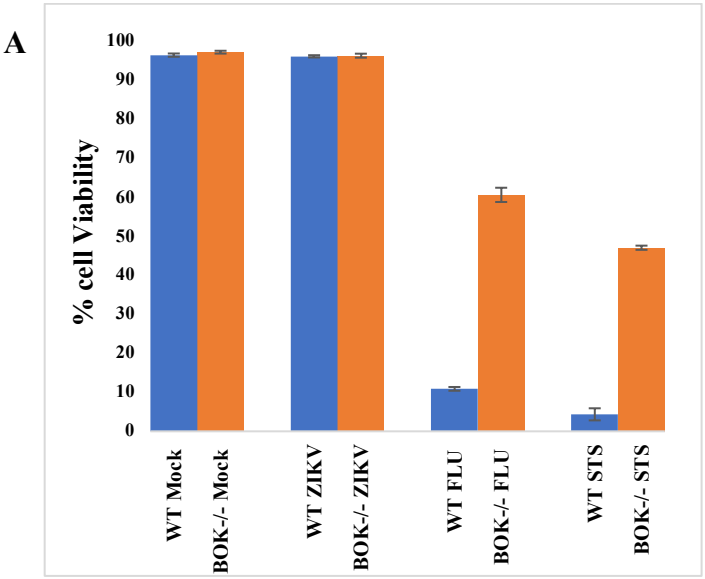

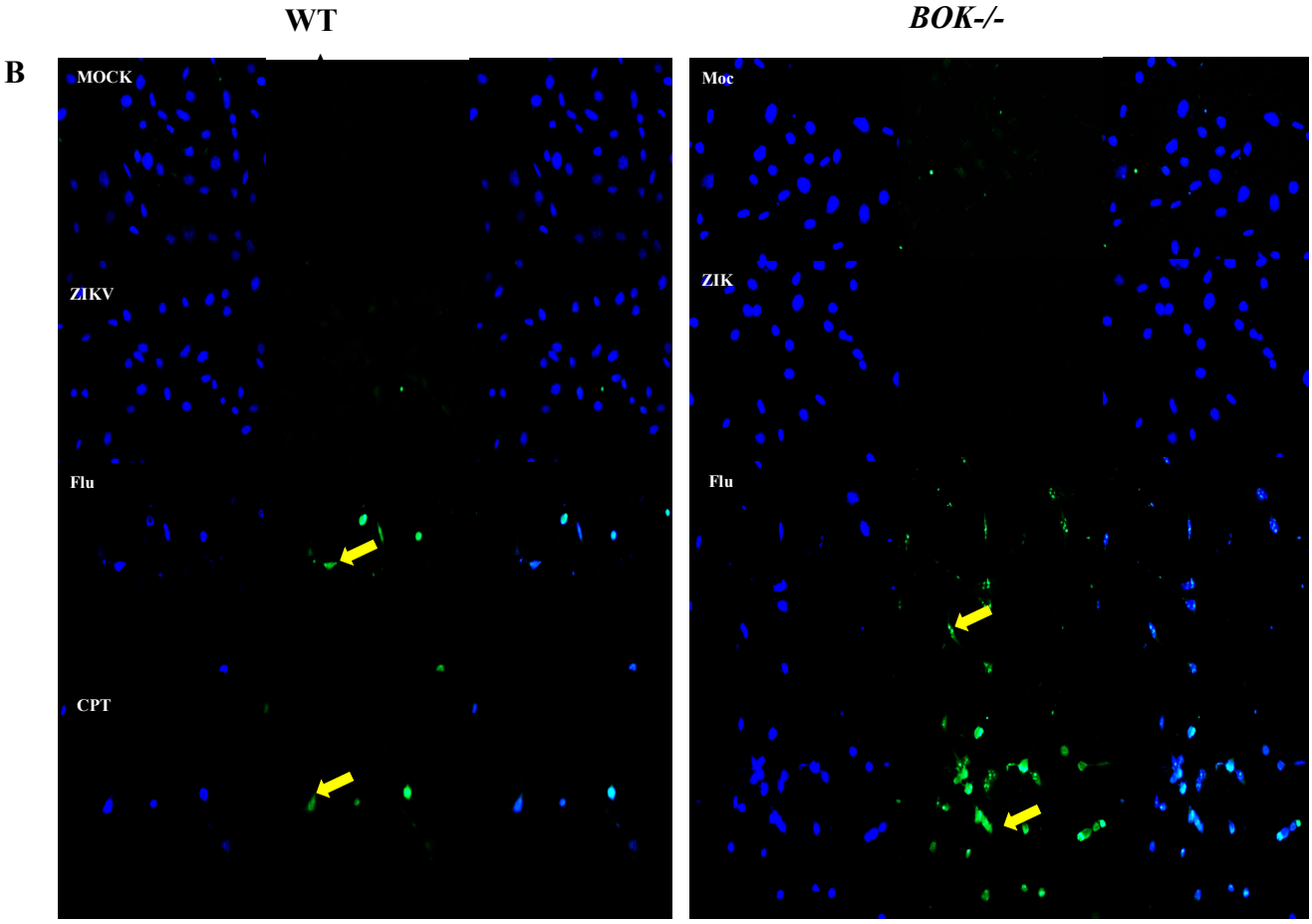

Figure 7: A. MEFs were infected with ZIKV/Flu or treated with STS (5mM) for 24 hours and then cell viability was measured by trypan blue assay. ZIKV does not kill WT or *BOK*$^{-/-}$ cells. Flu and STS induce apoptosis in WT and *BOK*$^{-/-}$. **B.** These results were confirmed by immunofluorescence for cleavage of caspase 3. Cleavage of caspase 3 was detected in the Flu infected and STS WT and *BOK*$^{-/-}$ (yellow arrows). DAPI was used for nuclei staining.

Figure 8: Elimination of *BOK*$^{-/-}$ permits expression of virus

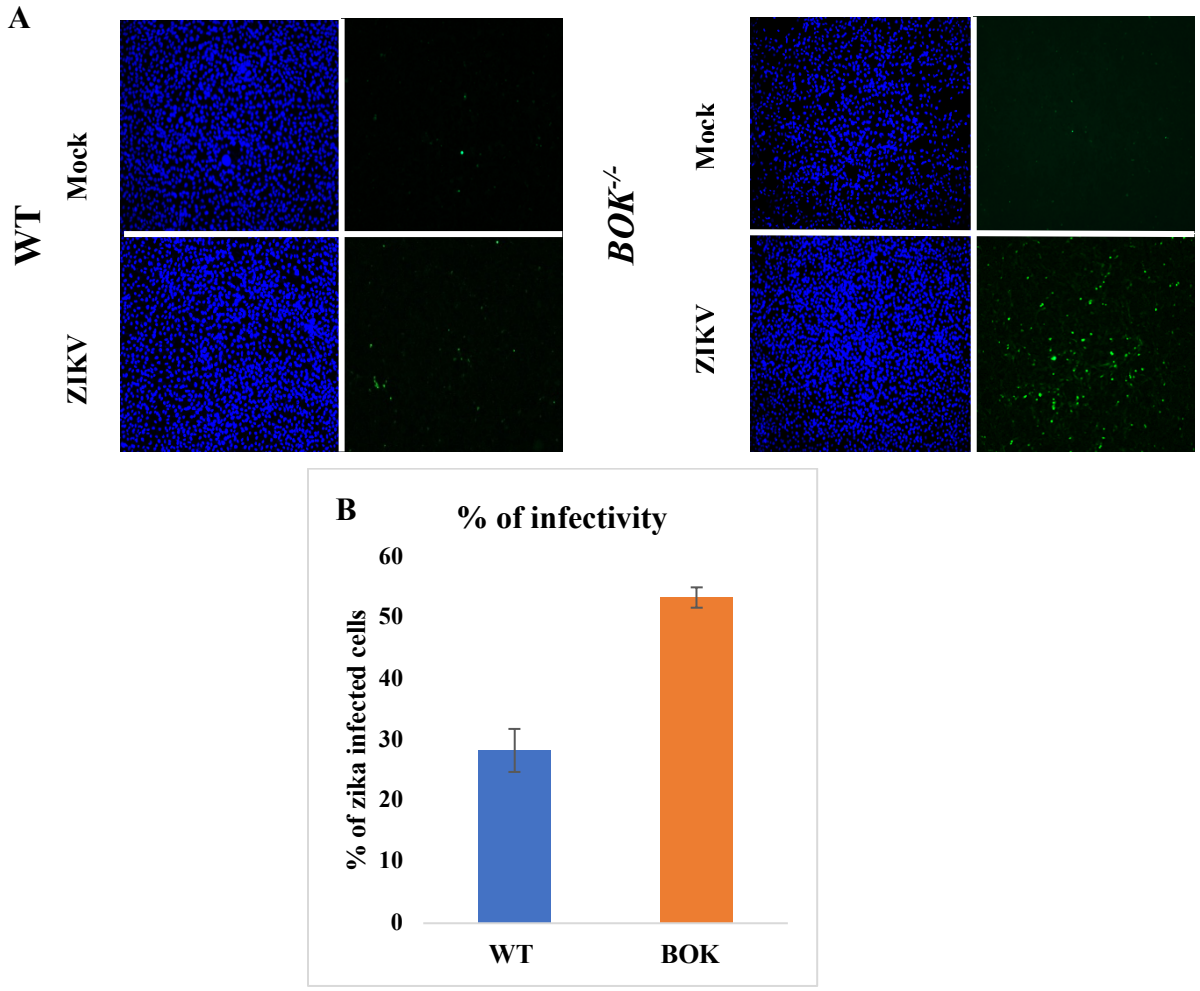

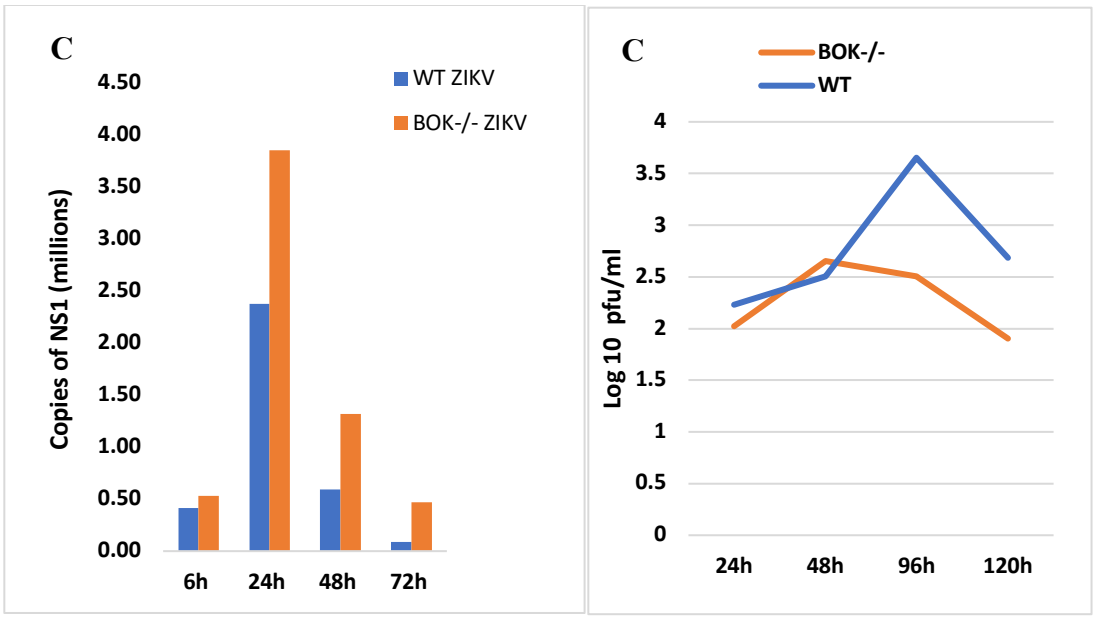

Figure 8: A. WT and *BOK*$^{-/-}$ MEFs' cells were infected with ZIKV for 24 h followed by measurement of immunofluorescence. The expression of the envelope protein was detected in the ZIKV-infected cells (green). DAPI was used for nuclei staining. **B.** The percentage of infectivity was calculated by counting the cells that present green signal (E protein) over the total number of cells. WT have low infectivity (25%) compared with the *BOK*$^{-/-}$ cell (53%). **C.** Viral RNA was extracted from infected cells at different times and NS1 was amplified. Fold change was calculated by the following equation: 2^([dCt]), when dCt<0, or −1(2) ^ ([dCt]), when dCt>0, where dCt= difference between Ct values. **D.** Viral reproduction was measured by plaque assay. The supernatant of infected cells was used to do a serial dilution and infect monolayers of Vero cells. WT released more virus particles than *BOK*$^{-/-}$ cells. In spite of infectivity of WT and *BOK*$^{-/-}$ (~25% and 50% with MOI of 5), we detected relatively few virus (in the range of 100-10,000 PFU/mL) suggesting that the mouse embryonic fibroblasts are efficiently infected

but with limited capacity to produce viral progeny and that they are less capable of producing virus when they lack BOK.